The blue shift of the optical absorption edge in ?-MnS

Article *in* Journal of Physics C Solid State Physics · October 1980

DOI: 10.1088/0022-3719/13/30/024

CITATIONS
20

READS
38

5 authors, including:

Katsuaki Sato
Tokyo University of Agriculture and Technology
289 PUBLICATIONS **3,491** CITATIONS

SEE PROFILE

J. Phys. C: Solid St. Phys., 13 (1980) 5615–29. Printed in Great Britain

The blue shift of the optical absorption edge in α-MnS

H Terasawa†, T Kambara†, K I Gondaira†, T Teranishi‡ and K Sato‡

† Department of Engineering Physics, The University of Electro-Communications, Chofu, Tokyo 182, Japan

‡ Broadcasting Science Research Laboratories of Nippon Hoso Kyokai, Kinuta, Tokyo 157, Japan

Received 19 March 1980

Abstract. The effect of antiferromagnetic ordering on the optical absorption edge in α-MnS is studied experimentally and theoretically. The absorption edge (3·33 eV) is conclusively determined from the dispersion of the interference fringe in a thin platelet crystal. The edge shows a blue shift of 0·22 eV on decreasing the temperature from room temperature to 4·2 K. The electronic structures of MnS in both paramagnetic and antiferromagnetic phases are calculated by using the self-consistent-charge extended Hückel method in order to clarify the nature of the transition and the mechanism of the edge shift. The observed blue shift can be reasonably explained by a model which attributes the edge to a transition corresponding to the magnetic exciton constructed with a hole in the 3d orbitals and an electron in the 4p orbitals of Mn ions.

1. Introduction

One of the interesting properties of transition-metal chalcogenides is that the optical absorption edge shifts markedly as the temperature is decreased below the Néel temperature. For the antiferromagnetic MnS, in particular, optical measurements near the absorption edge have been actively carried out (Huffman and Wild 1967, Teranishi and Sato 1970, Chou and Fan 1974). It has been observed that the absorption edge near 3 eV at room temperature shifts towards the short-wavelength by a few tenths of eV below the Néel temperature $T_N = 150\,\mathrm{K}$; that is, the blue shift is observed. It should be noted that this is a remarkably large observed shift, of the order of a magnitude or more larger than the ordinary magnetic ordering energies ($\sim kT_N$).

Huffman and Wild (1967) interpreted the absorption edge as arising from charge transfer transitions from the valence band consisting of mainly S 3p to empty 3d levels of Mn. They did not mention, however, the mechanism of the shift. Teranishi and Sato (1970) attributed the edge to transitions corresponding to the magnetic exciton which consists of a hole in 3d orbitals and an electron in a 4p orbital of Mn. Their suggestion about the mechanism of the edge shift was: when the wavefunction of final state, 4p of Mn mixed with 3p of S, spreads over the fourth-neighbour (see figure 5) Mn ions, the excitation energy below T_N increases due to the intra-atomic exchange interaction on those Mn sites, since in the antiferromagnetic structure of MnS the spins of all six fourth-neighbour Mn ions align antiparallel with that of the central Mn ion (Corliss *et al* 1956). Chou and Fan (1974) also assigned the absorption edge to the local transition

0022-3719/80/305615+15 $01.50

from the central Mn 3d orbitals to the orbitals consisting of the central Mn 4p orbitals and the neighbouring (second and fourth) Mn 4s orbitals, and gave the semiquantitative estimate of the edge shift taking into account the magnetostriction and the direct effects of the magnetic interactions. Nevertheless, we think the nature of the transition corresponding to the absorption edge, particularly that of the final state, has not yet been established. Whatever model one assumes for the final state, the conclusive theory should answer the questions: does such a localised state really exist in the crystal and is the calculated energy of the state consistent with the observed shift?

In order to clarify the nature of the transition and the mechanism of the edge shift, measurements were made firstly of the optical absorption spectrum of an α-MnS single crystal obtained by the chemical transport method. The precise determination of the absorption edge of this material was very difficult since the absorption edge has a long-wavelength tail which overlaps with the absorption band at 2·7 eV and is assigned to the crystal-field transition $^6A_1 \rightarrow {}^4A_1, {}^4E$ of Mn^{2+} ions. The absorption edge was conclusively determined from the dispersion of the interference fringe in a good thin platelet crystal. Measurements of the absorption spectra were made for temperatures down to 4·2 K through the Néel temperature and the temperature shift of the absorption edge originating in the magnetic effect was determined. Quantitative calculations of the electronic structure of MnS were then made. Since it seems reasonable to assign the edge to the local transition, the cluster model was adopted; the cluster contains 19 Mn ions up to the fourth neighbours of the central Mn ion. The electronic structure of the cluster in both paramagnetic and antiferromagnetic phases was calculated by the self-consistent-charge extended Hückel method which has been successfully used for transition-metal compounds. Finally the observed results were analysed on the basis of the calculated electronic structure.

2. Experimental results

Thin single-crystal platelets of α-MnS were grown by the chemical transport method. Conditions used were temperatures of 900 and 400 °C for the hot and cold ends of the growth tube respectively and 3 mg cm^{-3} of iodine as the transporter. A rather small amount of transporter was necessary to get a platelet with very perfect and parallel surfaces. The large faces were (111) planes. Optical absorption measurements were made with a Leiss single-beam double monochromator and a Cary 14 recording spectrophotometer from photon energies of about 0·6 to 3·1 eV.

The observed spectrum showed three absorption bands arising from crystal-field transitions at 2·03, 2·43, and 2·75 eV and a steep rise near 3 eV. Interference fringes were observed throughout the entire transmitting region in a good thin crystal. In figure 1 the fringe number m is plotted against the wavenumber f where the interference fringe appears. The fringe number 1 is assigned to the lowest energy fringe which we can observe. In an energy range lower than 15×10^3 cm^{-1}, the wavenumber f has a linear variation with fringe number:

$$f = m/(2nd) \tag{2.1}$$

where n is the refractive index and d is the thickness of the specimen. From this linear relation we obtain 10·2 μm as the thickness value of our crystal, inserting the value of the refractive index 2·69, which has been given by Huffman (1966) for α-MnS. The deviation from the linear relationship is not observed at lower energies where three absorption

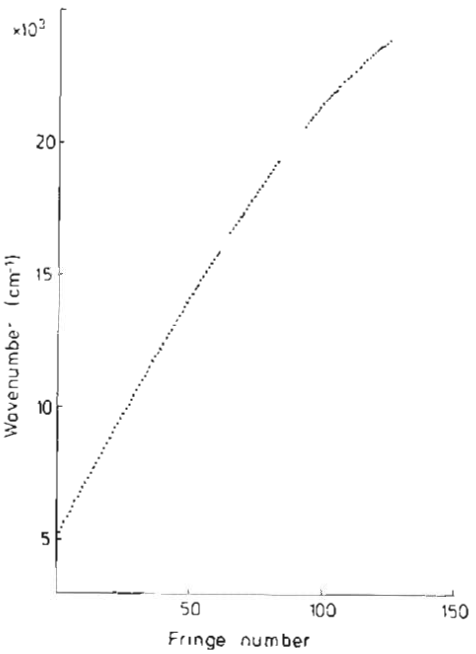

Figure 1. Plot of the energy where interference fringe appears against the fringe number. Measurements were made at room temperature.

bands appear. These absorptions are attributed to crystal-field transitions which are parity-forbidden and do not give any serious effect to the dispersion relation of the refractive index.

At an energy range higher than 15×10^3 cm^{-1} the linearity breaks. This results from the dispersion of the refractive index n as

$$n^2 = 1 + A/(f_0^2 - f^2) \tag{2.2}$$

where A and f_0 are constants. The damping term is dismissed because in this case the absorption which causes the dispersion of the refractive index may be attributed to a local transition. When f equals f_0, that is the refractive index disperses to infinity, an allowed transition occurs, giving an intense optical absorption. The observed absorption around 3 eV may be interpreted as an allowed transition that breaks the linear relationship between fringe number and wavenumber. Refractive indices were determined for the corresponding wavenumbers over the whole range of energy shown in figure 1, where the value 10·2 μm was used as the thickness of the crystal. The variation in refractive index with wavenumber may be approximated by equation (2.2) and the best fitting constants f_0 and A were determined by the method of least squares. Results are given in figure 2. Full circles represent the measured refractive indices varying with the energy and the full curve is the calculated best fit. The obtained values of f_0 and A are $2{\cdot}69 \times 10^4$ and $4{\cdot}52 \times 10^9$ cm^{-1}, respectively. It is therefore concluded that an allowed transition exists which makes the absorption edge at a photon energy $2{\cdot}69 \times 10^4$ cm^{-1} (3·33 eV).

The magnitude of the temperature shift of this transition was determined from the temperature variation of the absorption spectrum since the temperature-dependent

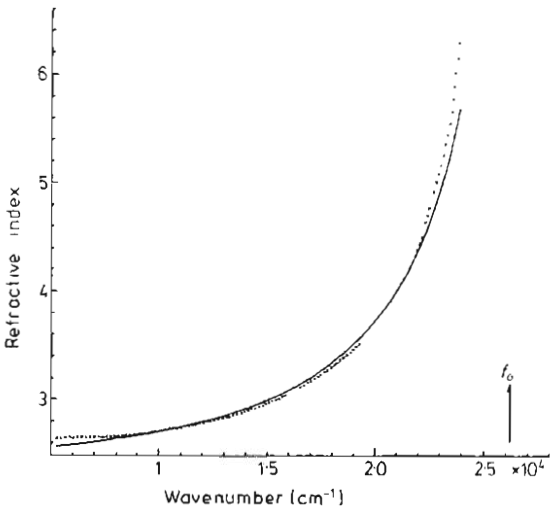

Figure 2. Dispersion of the refractive index. Dots are data points and the full curve is the calculated result.

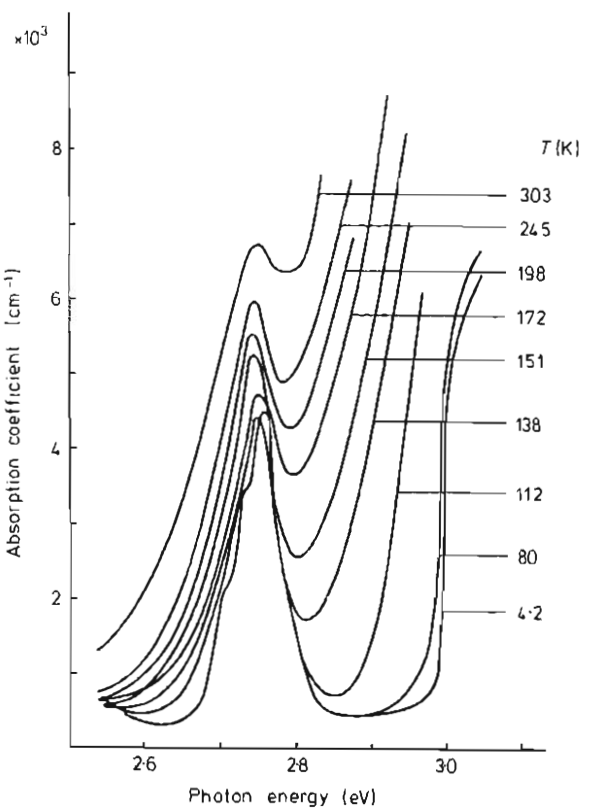

Figure 3. Optical absorption spectra at various temperatures.

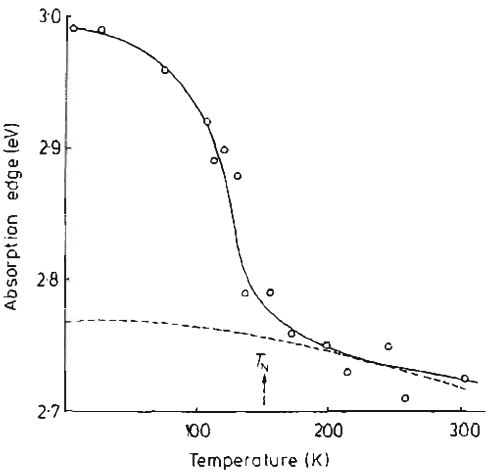

Figure 4. Shift of the absorption edge with temperature.

measurement of the dispersion of the refractive index was very difficult. Figure 3 shows the absorption spectra for various temperatures. In order to obtain the definite absorption edge from the spectrum, the part of absorption originating in the crystal-field transition $^6A_1 \rightarrow {}^4A_1, {}^4E$ was subtracted from the total absorption. The extrapolation of the resultant absorption spectrum was made to be linear down to the horizontal axis of zero absorption at every temperature. The intersecting point with the horizontal axis was regarded as an absorption edge. Figure 4 is a plot of the energy of the absorption edge against the absolute temperature. The broken curve was obtained by extrapolating the data for $T > 172$ K according to a T^2 variation. The difference between the extrapolated and the measured curve gives the effect of magnetic ordering and gives 0·22 eV at 0 K.

3. Theoretical model and method of calculation

3.1. Model

MnS is a type-II antiferromagnet, its structure changing from FCC (a = 5·2236 Å (Wyckoff 1963)) in the paramagnetic phase to trigonal (a' = 5·2137 Å, trigonal distortion angle $\Delta = 1{\cdot}72 \times 10^{-3}$ rad (Morosin 1970)) in the antiferromagnetic phase due to the magnetic exchange striction.

The cluster used in the present calculation is made up of a Mn ion and 62 neighbouring ions (6 first neighbour S, 12 second Mn, 8 third S, 6 fourth Mn, 24 fifth S and 6 eighth S). Effects of the remaining crystal on the cluster are taken into account as a crystal potential which is calculated in the point-change approximation. The cluster is shown in figure 5 in which all the ions are numbered as shown for later convenience. The symmetry of the cluster is O_h and the sets of equivalent ions are [Mn(1)], [S(2)–S(7)], [Mn(8)–Mn(19)], [S(20)–S(27)], [Mn(28)–Mn(33)], [S(34)–S(57)] and [S(58)–S(63)] in the paramagnetic phase. The symmetry is D_{3d} and the sets of equivalent ions are [Mn(1):↑], [S(2)–S(7)], [Mn(8)–Mn(13):↓], [Mn(14)–Mn(19):↑], [S(20)–S(21)], [S(22)–S(27)], [Mn(28)–Mn(33):↓], [S(34)–S(45)], [S(46)–S(57)] and [S(58)–S(63)] in the antiferromagnetic phase. In figure 5, the shaded Mn ions have down (↓) spins and the unshaded

ones have up (↑) spins in the antiferromagnetic phase. The spin polarisation of S ions is neglected throughout the present calculation.

The electronic wavefunctions extended over the whole cluster are expressed in terms of the linear combination of atomic basis orbitals. The basis orbitals are 3d, 4s, 4p for Mn and 3s, 3p for S. There are, in total, 347 distinct atomic orbitals of the 63 ions to be taken into account in the calculation. The charge of the cluster is assumed to be the value determined from the formal charge (Mn^{2+}, S^{2-}) of the component ions, and hence 447 electrons are explicitly considered.

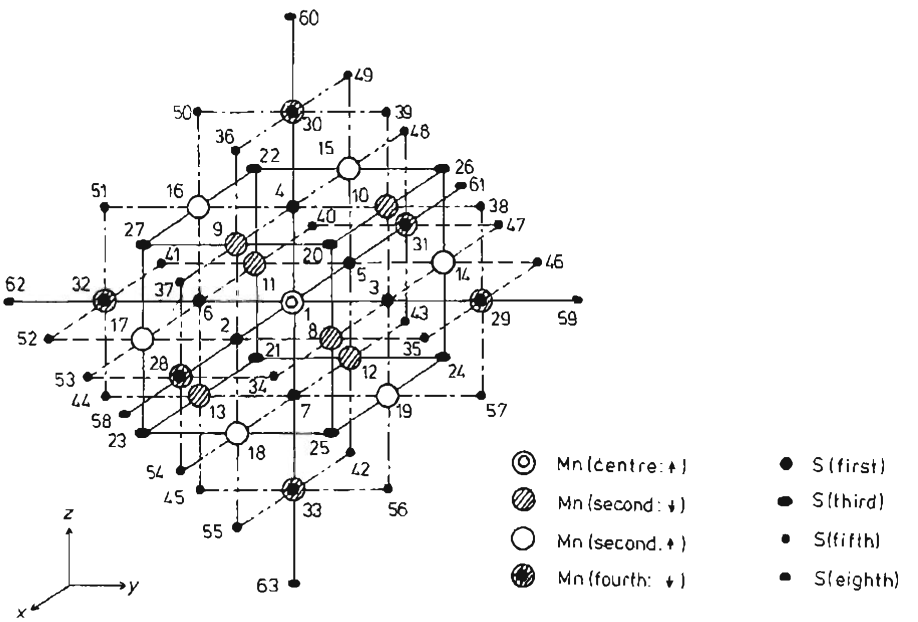

Figure 5. $Mn_{19}S_{44}$ cluster and the coordinate system.

The atomic orbital functions are taken from the table of Wachters (1970) for Mn 3d and from the table of McWilliams and Huzinaga (1975) for S 3s, 3p. Slater-type orbital functions are used for Mn 4s, 4p and their orbital exponents ζ are $\zeta_{4s} = 2{\cdot}0$ and $\zeta_{4p} = 1{\cdot}6$, which are obtained from the table of Burns (1964) by using the valency of Mn ion determined so as to reproduce the observed energy 6·2 eV (Huffman and Wild 1967) of the fundamental absorption edge.

3.2. Method of calculation

In order to calculate the electronic structure of the cluster, we use the unrestricted extended Hückel method, where different molecular orbitals are arranged for electrons with different spins. The eigenfunctions of the system are classified according to the irreducible representations of point groups, O_h and D_{3d}, in the paramagnetic phase and in the antiferromagnetic phase, respectively. The pth molecular orbital of symmetry Γ for an α-spin

electron is represented as

$$\Psi^{\alpha}_{\Gamma p} = \sum_{n} C^{\alpha}_{np}(\Gamma)\chi_{\Gamma n} \tag{3.1}$$

where $\chi_{\Gamma n}$ is the nth symmetrised linear combination of equivalent atomic orbitals.

The coefficients $C^{\alpha}_{np}(\Gamma)$ and eigenvalues $E^{\alpha}_{p}(\Gamma)$ are obtained by solving following equations iteratively until the self-consistent charge is attained for each ion:

$$\mathbf{H}^{\alpha}(\Gamma)\mathbf{C}^{\alpha}(\Gamma) = \mathbf{G}(\Gamma)\mathbf{C}^{\alpha}(\Gamma)\mathbf{E}^{\alpha}(\Gamma) \tag{3.2}$$

where

$$H^{\alpha}_{mn}(\Gamma) = \langle \chi_{\Gamma m} | H^{\alpha} | \chi_{\Gamma n} \rangle \tag{3.3}$$

$$G_{mn}(\Gamma) = \langle \chi_{\Gamma m} | \chi_{\Gamma n} \rangle \tag{3.4}$$

$$E^{\alpha}_{pq}(\Gamma) = E^{\alpha}_{p}(\Gamma)\delta_{pq} \tag{3.5}$$

H^{α} being the one-electron Hamiltonian for α spin. The matrix elements (3.3), (3.4) are rewritten in terms of the matrix elements based on the atomic orbitals ϕ_i

$$h^{\alpha}_{ij} = \langle \phi_i | H^{\alpha} | \phi_j \rangle \tag{3.6}$$

$$S_{ij} = \langle \phi_i | \phi_j \rangle. \tag{3.7}$$

In equation (3.6), the diagonal terms are evaluated as

$$h^{\alpha}_{ii} = -V_{\mathrm{I}i} + V_{\mathrm{M}i} + V^{\alpha}_{\mathrm{S}i} \tag{3.8}$$

where V_{Ii} is the spin-independent ionisation energy for an electron in the atomic orbital ϕ_i, V_{Mi} is the crystal potential energy and V^{α}_{Si} represents the orbital energy change due to the spin polarisation. V^{α}_{Si} is taken into account only for Mn 3d in the paramagnetic phase and for Mn 3d, 4s, 4p in the antiferromagnetic phase. The off-diagonal terms are approximated by the method of Cusachs (1965) as

$$h^{\alpha}_{ij} = \tfrac{1}{2}S_{ij}(2 - |S_{ij}|)(h^{\alpha}_{ii} + h^{\alpha}_{jj}). \tag{3.9}$$

We adopt the expression of Basch *et al* (1966) for V_{Ii} of Mn

$$V_{\mathrm{I}i} = A_i q^2_{\mathrm{Mn}} + B_i q_{\mathrm{Mn}} + C_i, \tag{3.10}$$

and that of Carrol *et al* (1966) for S

$$V_{\mathrm{I}i} = D_i(\mathrm{POP})_i + B_i q_{\mathrm{S}} + C_i \tag{3.11}$$

where q_{Mn} is the charge on the Mn ion to which the atomic orbital ϕ_i belongs and $(\mathrm{POP})_i$ is the population in the atomic orbital ϕ_i. As shown later, the charges on the S ions on the cluster surface are considerably different from the charges on the inner S ions. The cluster surface being unreal, we take the charge on the inner S ions as q_S for the surface S ions. It is seen from table 2 of Basch *et al* (1966) that the parameters A_i, B_i, C_i for Mn 3d orbitals depend seriously on the electronic configuration. In the crystal, the population of very delocalised orbitals such as 4s and 4p of Mn do not have definite meaning and we cannot rigorously decide what configuration should be chosen in order to obtain the ionisation potential from that table. Therefore we have calculated the energy levels of the cluster in the paramagnetic phase using the parameters A_i, B_i, C_i of the Mn 3d orbitals for several configurations $\mathrm{d}^{7-q-x}\mathrm{S}^{x}\mathrm{P}^{0}$ $(1{\cdot}5 > x > 0)$ where q is

the self-consistent charge of Mn. We show the results for the two cases corresponding to the configurations $d^{5.5}\,s^{1.0}$ (I) and $d^{6.2}\,s^{0.3}$ (II). It will be shown later that the calculated energy levels for cases I ($d^{5.5}\,s^{1\,0}$) and II ($d^{6.2}\,s^{0.3}$) favour the charge transfer model (Huffman and Wild 1967) and the magnetic exciton model (Teranishi and Sato 1970) for optical absorption edge, respectively. The parameters A_i, B_i, C_i, D_i are listed in table 1, where the values for d orbitals in case II (non-integral occupation of s) are evaluated by $X_i = 0.3\,X_i(d^{n-1}\,S^1) + 0.7\,X_i(d^n)$ (X = A, B, C).

Table 1. The parameters A_i, B_i, C_i and D_i of ionisation potentials for Mn and S (in eV).

Mn orbitals	A_i	B_i	C_i	S orbitals	D_i	B_i	C_i
3d I	0·68	13·0	7·95	3s	−2·43	9·7	26·15
II	1·43	10·9	5·73	3p	−1·12	9·7	13·62
4s	0·94	7·55	6·86				
4p	0·89	6·11	3·62				

As the crystal potential energy V_{Mi} for relatively localised atomic orbitals such as Mn 3d and S 3s, 3p, we use the Madelung potential of each ion to which the atomic orbital ϕ_i belongs,

$$V_{Mi} = +\alpha q e^2/R_0 \qquad \text{for Mn} \tag{3.12}$$

$$= -\alpha q e^2/R_0 \qquad \text{for S} \tag{3.13}$$

where α is the Madelung constant, q is the average of q_{Mn} for the central Mn and q_S for the nearest neighbouring S, and R_0 is the nearest neighbour distance. We take zero for V_{Mi} of the delocalised orbitals, Mn 4s, 4p, since electrons in these orbitals can be assumed to see the averaged crystal potential.

Slater (1968) represents the difference between the one-electron energies with spin up and spin down in terms of the Slater–Condon parameters. By using the value of those parameters given by Hinze and Jaffe (1963), V_{Si} is written as

$$V^{\alpha}_{S3d} = -(n_\alpha - n_\beta)0.3658\ \text{eV} \tag{3.14}$$

$$V^{\alpha}_{S4s} = -(n_\alpha - n_\beta)0.0807\ \text{eV} \tag{3.15}$$

$$V^{\alpha}_{S4p} = -(n_\alpha - n_\beta)0.2214\ \text{eV} \tag{3.16}$$

where n_α and n_β are the numbers of electrons in Mn 3d orbitals with α spin and β spin, respectively. The intra-atomic exchange interaction is so effective on the localised Mn 3d orbital that all of these orbitals are singly occupied and the electron spins are coupled to make the multiplicity of the ion maximum, even in the paramagnetic phase. On the other hand, Mn 4s, 4p orbitals extend to the neighbouring Mn ions, and electrons in these orbitals see an averaged exchange potential. Although atomic multiplets or intra-atomic exchange effects do not have a rigorous meaning in our calculation, since our treatment is based on the one-electron molecular orbital theory but not on the Heitler–London scheme, one can reasonably treat the intra-atomic exchange correlation effects within the one-electron scheme in the following way. The spin polarisation of Mn 3d are only taken into account in the paramagnetic phase by assuming a 'fictitious ferromagnetic' ordering of Mn spins, while the spin polarisation of Mn 3d, 4s, 4p are

taken into account in the antiferromagnetic phase. The assumption of the 'fictitious ferromagnetic' ordering accompanies undesirable effects of the inter-atomic exchange which certainly do not appear in the paramagnetic phase. These spurious effects are insignificant in the present problem, since their order of magnitude is, at most, 100 cm^{-1} ($\sim kT_N$) and we are concerned mainly with an energy shift of several thousands cm^{-1} which is, however, triggered by the occurrence of the magnetic ordering but results from a much larger effect, the intra-atomic exchange effect.

4. Calculated results

4.1. Results in case I

In this subsection, we present the results in case I, where the values of A_i, B_i, C_i for Mn 3d correspond to the configuration $d^{5.5}$ $s^{1.0}$ of Mn. This configuration is adopted as a representative of the configurations for which the occupied energy levels arising from Mn 3d orbitals is close to the valence band arising from S 3p orbitals. In this case the resultant position of 3dϵ levels is rather sensitive to the configuration.

The self-consistent charges and electron configurations of each inequivalent ion are presented in table 2 for both the paramagnetic and antiferromagnetic phase. The self-consistency of the charges is attained within 0·01 *e* in the paramagnetic phase, while the larger calculation for the antiferromagnetic phase is done to an accuracy of within 0·05*e* except for the charge of Mn(1) to save machine time.

Table. 2. The self-consistent charges and the electron configurations in case I.

Phase	Ion	Charge	3dϵ	3dγ	4s	4p	Ion	Charge	3s	3p
Para-magnetic	Mn(1)	0·48	↑3·00	1·98	0·36	0·37	S(2)	−0·61	0·91	2·43
			↓0·01	0·12	0·33	0·35			0·91	2·45
	Mn(8)	0·44	↑3·00	1·99	0·34	0·39	S(20)	−1·18	0·95	2·68
			↓0·01	0·12	0·33	0·38			0·94	2·61
	Mn(28)	0·42	↑3·00	2·00	0·34	0·39	S(34)	−1·45	0·96	2·79
			↓0·01	0·12	0·33	0·39			0·96	2·74
							S(58)	−1·73	0·98	2·90
									0·98	2·87
Antiferro-magnetic†	Mn(1)	0·26	↑3·00	1·97	0·36	0·55	S(2)	−0·56	0·91	2·38
			↓0·02	0·18	0·33	0·34			0·91	2·38
	Mn(8)	0·42	↑0·02	0·14	0·32	0·28	S(20)	−1·17	0·95	2·66
			↓3·00	1·99	0·35	0·49			0·94	2·62
	Mn(14)	0·41	↑3·00	1·98	0·35	0·49	S(22)	−1·17	0·94	2·63
			↓0·02	0·14	0·32	0·28			0·95	2·65
	Mn(28)	0·41	↑0·02	0·13	0·32	0·29	S(34)	−1·44	0·97	2·77
			↓3·00	1·99	0·35	0·50			0·95	2·75
							S(46)	−1·44	0·96	2·76
									0·96	2·76
							S(58)	−1·72	0·98	2·89
									0·97	2·88

† The occupation numbers of the relevant orbitals are shown to the order of 0·01, although the last figure might not be very meaningful for the antiferromagnetic phase because of a possible error of 0·05.

The charges and electron population of Mn orbitals are not different between inequivalent Mn ions in the paramagnetic phase. The Mn 3dϵ, 3dγ orbitals for up spin are fully occupied and the Mn 4s, 4p orbitals are equally occupied by up and down spin electrons, as expected from our assumption of fictitious ferromagnetic ordering in the paramagnetic phase. In the antiferromagnetic phase, the spin polarisation of Mn ions is up for Mn(1) and Mn(14) and down for Mn(8) and Mn(28), as expected. The electron population of Mn orbitals is almost equivalent to that for Mn(1) apart from the difference in the spin direction. The electron spins of the Mn 4s, 4p orbitals are slightly polarised in the same direction as that of the 3d orbitals of each Mn ion. On the other hand, the charges of S ions on the cluster surface are considerably different from the charge on the inner S(2) ion, since S(20), S(34), S(58) ions have only 3, 2 and 1 nearest neighbouring Mn ions, respectively. The large departure of the charge of each ion from the formal charge (Mn^{2+}, S^{2-}) shows that the covalency effect is important between Mn ions and S ions.

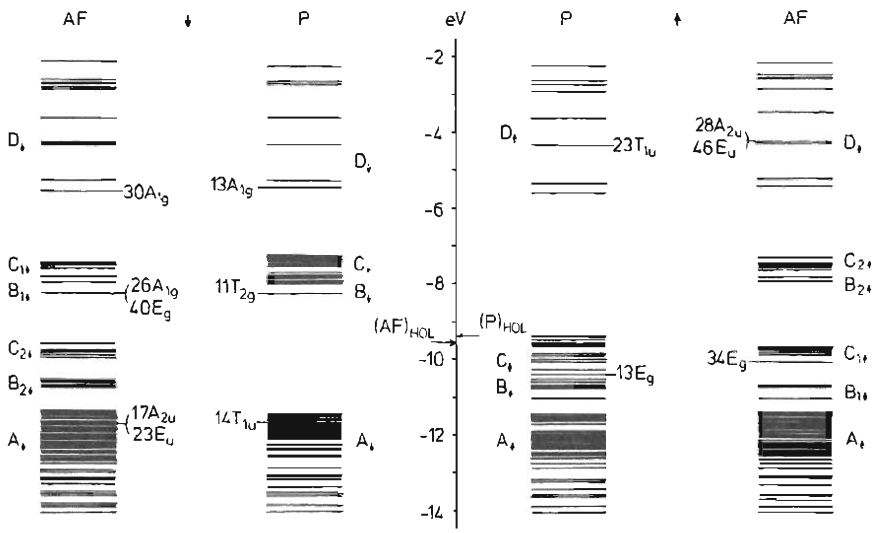

Figure 6. The calculated energy levels near the Fermi level in case I. The energies of the highest occupied levels in the paramagnetic $(P)_{HOL}$ and in the antiferromagnetic $(AF)_{HOL}$ phases are −9·38 and −9·56 eV, respectively.

The sets of energy levels are illustrated in figure 6. The inner two diagrams are for the paramagnetic phase and the outer two are for the antiferromagnetic phase. The two diagrams on the right-hand side and the two on the left hand side are for up and down spin electrons, respectively. The groups of levels $A_\uparrow$ and $A_\downarrow$ are composed predominantly of the S 3p orbitals and correspond to the valence band. There are other groups of levels composed of the S 3s orbitals between −22·7 and −21·2 eV in both phases. They are not shown in figure 6. The groups B and C are composed of mainly Mn 3dϵ and Mn 3dγ orbitals, respectively. In the antiferromagnetic phase, the subscript 1 of B and C denotes Mn ions with up spin (Mn(1), Mn(14)) and the subscript 2, Mn ions with down spin (Mn(8), Mn(28)). The groups of levels $D_\uparrow$ and $D_\downarrow$ are composed of the Mn 4s orbitals and these levels correspond to the conduction band. Above these levels, there are levels composed of the Mn 4p orbitals up to 1·8 eV in the paramagnetic phase and up to 3·2 eV in the antiferromagnetic phase. They are not shown in figure 6.

Table 3. The self-consistent charges and the electron configurations in case II.

Phase	Ion	Charge	$3d\epsilon$	$3d\gamma$	4s	4p	Ion	Charge	3s	3p
Para-magnetic	Mn(1)	0·50	↑3·00	1·95	0·40	0·40	S(2)	−0·63	0·91	2·41
			↓0·00	0·03	0·34	0·37			0·91	2·40
	Mn(8)	0·47	↑3·00	1·98	0·36	0·41	S(20)	−1·20	0·94	2·67
			↓0·00	0·03	0·35	0·40			0·94	2·65
	Mn(28)	0·46	↑3·00	1·99	0·35	0·42	S(34)	−1·46	0·96	2·78
			↓0·00	0·03	0·34	0·41			0·96	2·77
							S(58)	−1·73	0·98	2·89
									0·98	2·89
Antiferro-magnetic†	Mn(1)	0·32	↑3·00	1·95	0·39	0·58	S(2)	−0·60	0·90	2·40
			↓0·00	0·04	0·37	0·35			0·90	2·40
	Mn(8)	0·47	↑0·00	0·03	0·34	0·29	S(20)	−1·20	0·95	2·70
			↓3·00	1·97	0·37	0·52			0·93	2·61
	Mn(14)	0·47	↑3·00	1·97	0·37	0·53	S(22)	−1·19	0·94	2·64
			↓0·00	0·03	0·34	0·29			0·95	2·67
	Mn(28)	0·45	↑0·00	0·03	0·33	0·30	S(34)	−1·46	0·97	2·80
			↓3·00	1·98	0·37	0·54			0·95	2·74
							S(46)	−1·46	0·96	2·77
									0·96	2·77
							S(58)	−1·73	0·98	2·90
									0·97	2·87

† The occupation numbers of the relevant orbitals are shown to the order of 0·01, although the last figure might not be very meaningful for the antiferromagnetic phase because of a possible error of 0·05.

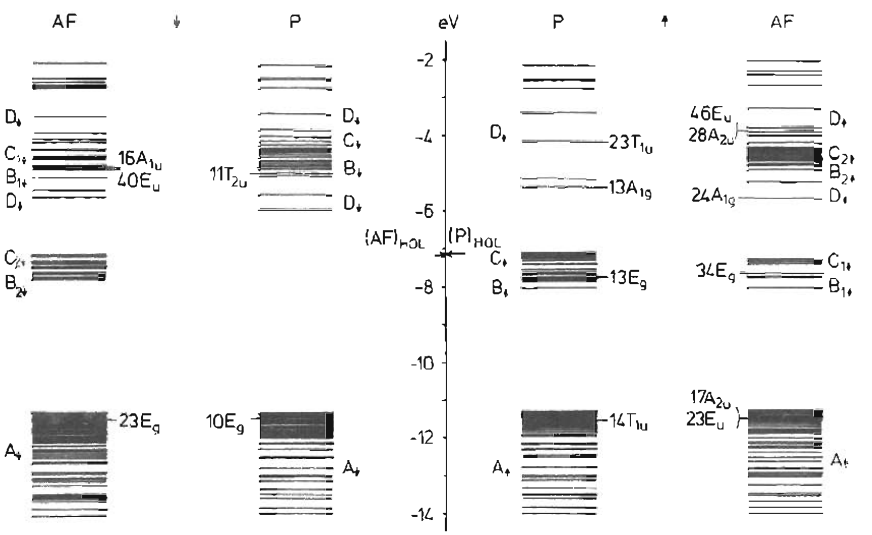

Figure 7. The calculated energy levels near the Fermi level in case II. $(P)_{HOL}$ is −7·11 and $(AF)_{HOL}$ is −7·16 eV.

4.2. Results in case II

In this subsection, we present the results for case II, where the values of A_i, B_i, C_i for Mn 3d correspond to the configuration $d^{6\cdot2}\,s^{0\cdot3}$ of Mn, other conditions being the same as in case I. In this case the occupied energy levels arising from Mn 3d orbitals are around the centre of the fundamental band gap. The resultant position of the levels is rather insensitive to the change of configuration as far as the occupied 3d levels are well separated from both the valence and the conduction bands.

The self-consistent charges and electron configurations of each inequivalent ion are presented in table 3. The major differences from the case I are as follows. The absolute value of the charge of each ion is slightly larger than the corresponding value for case I. This is because the energy separation between the Mn 3d orbitals and the S 3p is larger for case II than for case I.

The sets of energy levels are illustrated in figure 7. The energy diagram has a similar pattern to that in case I, but there are some differences arising from the energy of the Mn 3d orbitals. The width of the groups of levels B and C with up spin in the paramagnetic phase are narrower than those in case I. The groups of levels B and C, composed of essentially the Mn 3d orbitals, are shifted to higher energy by about 3 eV. The groups B and C for down spin in the paramagnetic phase, and their upper components in the antiferromagnetic phase, enter into the group of levels D, separating it into two parts.

Table 4. Some calculated transition energies and relevant energy levels in case II†

Phase	Transition (eV)		Symmetry	Orbital energy (eV)	Leading constituent atomic orbitals with their composition ratios (%)
Paramagnetic	FAE (6·20)	i	14 T_{1u}	−11·68	S(34) 3p:38, S(2) 3p:35, S(20) 3p:19
		f	13 A_{1g}	−5·48	Mn(1) 4s:28, Mn(28) 4s:17, Mn(8) 4s:15
	MET (6·07)	i	13 E_g	−10·40	Mn(1) 3dγ:41, Mn(28) 3dγ:21
		f	23 T_{1u}	−4·33	Mn(28) 4s:37, Mn(8) 4s:23, S(34) 3p:15
	CTT (3·43)	i	14 T_{1u}	−11·68	S(34) 3p: 38, S(2) 3p:35
		f	11 T_{2g}	−8·25	Mn(1) 3dε:99
Antiferromagnetic	FAE (6.17)	i	23 E_u	−11·71	S(46) 3p:39, S(34) 3p:30, S(2) 3p:9
			17 A_{2u}	−11·70	S(46) 3p:41, S(34) 3p:18, S(2) 3p:14
		f	30 A_{1g}	−5·54	Mn(1) 4s:30, Mn(28) 4s:18
	MET (5·84)	i	34 E_g	−10·08	Mn(1) 3dγ:57, S(2) 3p:24
		f	46 E_u	−4·24	Mn(8) 4s:48, Mn(28) 4s:12
			28 A_{2u}	−4·24	Mn(28) 4s:37, Mn(8) 4s:24
	CTT (3·46)	i	23 E_u	−11·71	S(46) 3p:39, S(34) 3p·30
			17 A_{2u}	−11·70	S(46) 3p:41, S(34) 3p:18
		f	40 E_g	−8·24	Mn(1) 3dε:99
			26 A_{1g}	−8·24	Mn(1) 3dε:99

† In tables 4 and 5 FAE, MET and CTT mean the fundamental absorption edge, the magnetic exciton transition and the charge transfer transition, respectively, and i and f denote the initial and final states for the relevant transition, respectively.

5. Analysis of the absorption edge

The resulting transition energies corresponding to the fundamental absorption edge, the magnetic exciton transition and the charge transfer transition are listed in tables 4 and 5 for case I and II, respectively, with the orbital energies and some leading constituent atomic orbitals of the relevant levels.

In case I, the fundamental absorption edge is assigned to the transition from 14 T_{1u} ($-11{\cdot}68$ eV), the highest valence band level including, significantly, the S(2) 3p orbitals, to 13 A_{1g} ($-5{\cdot}48$ eV), the lowest conduction band level, in the paramagnetic phase, the transition energy of which is fitted to the observed value 6·2 eV as mentioned in § 3. In the antiferromagnetic phase, the fundamental absorption edge is assigned to the transition from the two levels, 23 E_u ($-11{\cdot}71$ eV) and 17 A_{2u} ($-11{\cdot}70$ eV), splitting from 14 T_{1u} to 30 A_{1g} ($-5{\cdot}54$ eV) and the transition energy is 6·17 eV. Several absorption peaks of lower transition energies than the fundamental absorption edge are expected, in which the Mn 3d levels take part. First of all, the transition from 13 E_g ($-10{\cdot}40$ eV) to 23 T_{1u} ($-4{\cdot}33$ eV) in the paramagnetic phase corresponds to the magnetic exciton model (Teranishi and Sato 1970); 13 E_g is fairly localised on the centre Mn and the 23 T_{1u} state is well localised on the fourth neighbour Mn. However, its transition energy 6·07 eV

Table 5. Some calculated transition energies and relevant energy levels in case II†

Phase	Transition (eV)		Symmetry	Orbital energy (eV)	Leading constituent atomic orbitals with their composition ratios (%)
Paramagnetic	FAE (6.17)	i	14 T_{1u}	−11·56	S(2) 3p:37, S(34) 3p:32, S(20) 3p:22
		f	13 A_{1g}	−5·39	Mn(1) 4s:27, Mn(28) 4s:17, Mn(8) 4s:15
	MET	i	13 E_g	−7·76	Mn(8) 3dε:48, Mn(1) 3dγ:32
	(3·57)	f	23 T_{1u}	−4·19	Mn(28) 4s:37, Mn(8) 4s:22, S(34) 3p:16
	CTT	i	10 E_g	−11·48	S(34) 3p:49, S(2) 3p:28, S(58) 3p:18
	(6·48)	f	11 T_{2u}	−5·00	Mn(8) 3dγ:49, Mn(8) 4s:23, Mn(8) 3dε:9
Antiferro-magnetic	FAE (5·80)	i	23 E_u	−11·51	S(34) 3p:38, S(46) 3p:35, S(58) 3p:21, S(2) 3p:1
			17 A_{2u}	−11·50	S(58) 3p:28, S(2) 3p:24, S(20) 3p:18, S(34) 3p:13
		f	24 A_{1g}	−5·70	Mn(1) 4s:27, Mn(28) 4s:13
	MET	i	34 E_g	−7·67	Mn(1) 3dγ:76, Mn(14) 3dε:10
	(3·72)	f	28 A_{2u}	−3·96	Mn(28) 4s:28, Mn(8) 4s:19, Mn(8) 3dγ:16
			46 E_u	−3·94	Mn(8) 4s:29, Mn(8) 3dγ:15, Mn(28) 3dγ:14, Mn(14) 4s:11
	CTT	i	23 E_g	−11·51	S(34) 3p:34, S(58) 3p:28, S(46) 3p:20, S(22) 3p:10
	(6·65)	f	40 E_u	−4·88	Mn(14) 3dγ:44, Mn(14) 3dε:27, Mn(8) 4s:14
			16 A_{1u}	−4·82	Mn(14) 3dε:97

† See footnote to table 4 for an explanation of the symbols.

is considerably larger than the observed energy 3·33 eV. In the antiferromagnetic phase, the magnetic exciton transition corresponds to the transition from 34 E_g (−10·08 eV) to the two levels, 46 E_u (−4·24 eV) and 28 A_{2u} (−4·24 eV), arising from 23 T_{1u}, and the transition energy is 5·83 eV decreased by 0·24 eV due to the magnetic ordering. The transition from 14 T_{1u} (−11·68 eV) to 11 T_{2g} (−8·25 eV), the lowest unoccupied Mn 3d level, in the paramagnetic phase corresponds to the charge transfer model (Huffman and Wild 1967) and the transition energy 3·43 eV seems to be consistent with the observed energy. In the antiferromagnetic phase, the charge transfer transition corresponds to the transition from the two levels, 23 E_u (−11·71 eV) and 17 A_{2u} (−11·70 eV), splitting from 14 T_{1u}, to the two levels, 40 E_g (−8·24 eV) and 26 A_{1g} (−8·24 eV), arising from 11 T_{2g}, and the transition energy is 3·46 eV increased by 0·03 eV, very much smaller than the observed blue shift, 0·22 eV (present work), 0·097 eV (Chou and Fan 1974). In addition, the orbital energy of Mn 3d is much increased ($\simeq$ 10 eV) by the electron transfer due to the intra-atomic correlation effect, not included in the present calculation, so that the agreement of the calculated transition energy does not seem meaningful.

In case II, as shown in table 5, the fundamental absorption edge, in the paramagnetic phase, is assigned to the transition from 14 T_{1u} (−11·56 eV), the highest valence band level including, significantly, the S(2) 3p orbitals, to 13 A_{1g} (−5·39 eV), the lowest conduction band level, and the transition energy is fitted to the observed value. In the antiferromagnetic phase, the fundamental absorption edge is assigned to the transition from the two levels, 23 E_u (−11·51 eV) and 17 A_{2u} (−11·50 eV), splitting from 14 T_{1u}, to 24 A_{1g} (−5·70 eV) and the transition energy is 5·80 eV decreased by 0·37 eV. Among the transitions in which the Mn 3d levels take part, the transition from 13 E_g (−7·76 eV) to 23 T_{1u} (−4·19 eV) in the paramagnetic phase corresponds to the magnetic exciton transition. In this case, its transition energy 3·57 eV is consistent with the observed energy. In the antiferromagnetic phase, the magnetic exciton transition corresponds to the transition from 34 E_g (−7·67 eV) to the two levels, 28 A_{2u} (−3·96 eV) and 46 E_u (−3·94 eV). The transition energy is 3·72 eV increased by 0·15 eV and fairly consistent with the observed blue shift. The energy of the final state increases by 0·24 eV mainly due to the exchange splitting as expected in the magnetic exciton model. On the other hand, the energy of the initial state also increases by 0·09 eV mainly due to the magnetostriction of the crystal. The shift of the transition energy is the difference between these two values. The calculated amount of the blue shift is quite insensitive to the change of the configuration $d^{6\cdot2-x}s^{0\cdot3+x}$ ($|x| \leqslant 0{\cdot}1$) adopted for the ionisation potential of the Mn 3d orbital; the energies of the initial and final states are slightly dependent on the configuration. Even though the intra-atomic correlation effect on the final state is taken into consideration, the transition energy would not be greatly changed, because the main component, 4s of Mn, constituting the final state into which an electron is transferred is so delocalised. The transition from the highest valence band level 10 E_g (−11·48 eV) with down spin including, significantly, the S(2) 3p orbitals to the lowest unoccupied Mn 3d level 11 T_{2u} (−5·00 eV), corresponds to the charge transfer transition in the paramagnetic phase. Its transition energy 6·48 eV is considerably larger than the observed energy in contrast to case I. The corresponding charge transfer transition in the antiferromagnetic phase is that from 23 E_g (−11·51 eV) to the two levels, 40 E_u (−4·88 eV) and 16 A_{1u} (−4·82 eV) and the transition energy is 6·65 eV increased by 0·17 eV.

In conclusion, two typical cases, I and II, like those discussed here, make little difference to the fundamental absorption edge in which the 3d levels of Mn take no essential part. The magnetic exciton (ME) and the charge transfer (CT) transitions appear in both cases I and II, and the characteristic features of the initial and the final states of each

transition are essentially the same in both cases. The transition energies and their shifts due to magnetic ordering, however, are substantially different between the two cases. The transition energy of either the CT in case I or the ME in case II is consistent with the observed edge, but it is the ME in case II that shows a large blue shift comparable with that of the observed edge, which is substantially larger than the energy related to magnetic ordering although it is triggered by magnetic ordering. Furthermore, the transition energy, and particularly its shift due to the magnetic ordering in case II, are very stable in the sense that they are quite insensitive to slight variations of assumed electron configurations of Mn in the vicinity of the case $d^{6\cdot2}\,s^{0\cdot3}$. Judging from these features, the results in case II seems more realistic and it seems quite reasonable that the blue shifting absorption edge is assigned to the ME transition, in which the initial state wavefunction is localised on the 3d orbitals of a Mn ion, the wavefunction of the final state spreads over on the fourth neighbour Mn ions, and the blue shift occurs due to the intra-atomic exchange interaction on those Mn sites.

Acknowledgment

The authors wish to thank Mr M Uesugi for assitance in optical measurements.

References

Basch H, Viste A and Gray H B 1966 *J. Chem. Phys.* **44** 10–9
Burns G 1964 *J. Chem. Phys.* **41** 1521–2
Carrol D G, Armstrong A T and McGlynn S P 1966 *J. Chem. Phys.* **44** 1865–70
Chou H-h and Fan H Y 1974 *Phys. Rev.* **B10** 901–10
Corliss L, Elliot N and Hastings J 1956 *Phys. Rev.* **104** 924–8
Cusachs L C 1965 *J. Chem. Phys.* **43** S157–9
Hinze J and Jaffe H H 1963 *J. Chem. Phys.* **38** 1834–47
Huffman D R 1966 *PhD Thesis* University of California
Huffman D R and Wild R L 1967 *Phys. Rev.* **156** 989–97
McWilliams D and Huzinaga S 1975 *J. Chem. Phys.* **63** 4678–84
Morosin B 1970 *Phys. Rev.* **B1** 236–43
Slater J C 1968 *Phys. Rev.* **165** 658–69
Teranishi T and Sato K 1970 *Abstracts of 25th Annual Meeting of the Physical Society of Japan*, No. 3 p. 127 (in Japanese)
Wachters A J H 1970 *J. Chem. Phys.* **52** 1033–6
Wyckoff R W G 1963 *Crystal Structures* (New York: Wiley) vol 1 pp 85–94